Journal of ELECTRONIC MATERIALS, Vol. 42, No. 1, 2013
DOI: 10.1007/s11664-012-2263-7

Thermal Parameters, Microstructure, and Mechanical Properties of Directionally Solidified Sn-0.7 wt.%Cu Solder Alloys Containing 0 ppm to 1000 ppm Ni

BISMARCK LUIZ SILVA,[1] NOÉ CHEUNG,[2] AMAURI GARCIA,[3] and JOSÉ EDUARDO SPINELLI[1,4]

1.—Department of Materials Engineering, Federal University of São Carlos—UFSCar, São Carlos, SP 13565-905, Brazil. 2.—Federal Institute of Education, Science and Technology of São Paulo—IFSP, São João da Boa Vista, SP 13872-550, Brazil. 3.—Department of Materials Engineering, University of Campinas—UNICAMP, PO Box 6122 Campinas, SP 13083-970, Brazil. 4.—e-mail: spinelli@ufscar.br

Environmental concerns over the toxicity of Pb are resulting in the progressive ban of Pb-based solders as part of electrical and electronic devices. Sn-Cu alloys are becoming interesting Pb-free solder alternatives. In the case of hypoeutectic Sn-Cu alloys (< 0.7 wt.% Cu), small alloying additions of Ni can prevent the growth of coarse and deleterious Cu_6Sn_5 particles. Solidification thermal parameters such as the growth rate, cooling rate, and interfacial heat transfer coefficient (h_i) determine the morphology and scale of the phases forming the resulting microstructure. In the present study, directional solidification experiments were carried out with Sn-0.7 wt.%Cu, Sn-0.7 wt.% Cu-0.05 wt.%Ni, and Sn-0.7 wt.%Cu-0.1 wt.%Ni alloys and interrelations of solidification thermal parameters, microstructure, and tensile properties have been established. The highest time-dependent h_i profile was found for the Sn-0.7 wt.%Cu-0.1 wt.%Ni alloy, which is an indication that this alloy has the highest fluidity. Constrained dendritic arrangements were observed for all alloys experimentally examined. This morphology has been associated with high cooling rates and growth rates. Cellular regions, characterized by aligned eutectic colonies, were also observed to occur for cooling rates lower than 0.9 K/s and 6.0 K/s for the unmodified Sn-0.7 wt.%Cu alloy and for both Ni-modified Sn-Cu alloys, respectively. Experimental Hall–Petch-type equations correlating the ultimate tensile strength and elongation with cell/dendritic spacings are proposed.

Key words: Solidification, microstructure, thermal parameters, mechanical properties, solder alloys

INTRODUCTION

Soldering technology plays a key role in various levels of electronic packaging, such as solder joints in printed circuit boards (PCB) formed by either surface-mount soldering or plated through-hole (PTH) soldering of components, flip-chip connections, heat sink attachments, etc. The mechanical support in electronic packages depends on the solder joints. These joints serve as electrical interconnections as well. When either of these requirements cannot be met, the solder joint is considered to have failed, which can cause the collapse of the entire electronic system. Lead (Pb)-containing solders, such as 63Sn-37Pb, Pb-10Sn, and Pb-3Sn (all in wt.%), have been used in various microelectronic applications. Strong research and development efforts with a view to replacing Pb-containing solders with Pb-free solders are being

(Received June 12, 2012; accepted September 3, 2012; published online October 2, 2012)

made due to both competitive market pressures and environmental issues.[1–5]

Mainly due to cost concerns, the eutectic Sn-Cu alloy is becoming an interesting lead-free solder alternative.[6] Also, it has been successfully transferred to practical production. The Sn-Cu eutectic mixture is formed by the faceted eutectic Cu_6Sn_5 phase and the nonfaceted Sn-rich phase and occurs at 227°C.[7] The Cu_6Sn_5 phase grows in the form of rods embedded in a continuous Sn-rich matrix. One example of use of eutectic Sn-Cu alloy is that of the world's first virtually Pb-free telephone, where this alloy was chosen for both solder joints and surface finish layers of PCB and component termination pads.[8]

Unidirectional solidification systems can be very useful for understanding the evolution of microstructure in solder alloys. The technique can add useful information about the growth competition involving fine-scaled eutectic versus primary Sn dendrites or large brittle primary intermetallics for a single bulk composition. The comprehension of mechanisms responsible for the eventual prevalence of one of these features is of prime importance considering the final control of the solder fillet microstructure, as well as its mechanical properties and reliability. In general, the microstructure (morphology, scale, distribution) of Pb-free solders may be strongly influenced by altered growth conditions. For instance, transient-type directional solidification systems may permit free development of thermal solidification parameters (growth rate and cooling rate) during solidification, which is very similar to the conditions observed at industrial scale. Furthermore, thermal processing parameters play an important role in the final as-cast structure.[9–11] A recent investigation of a eutectic Sn-0.7 wt.%Cu solder alloy during transient solidification revealed that a gradual cellular to dendritic transition occurs for growth rates ranging from 0.3 mm/s to 0.5 mm/s. The cellular region was shown to be characterized by an alignment of two-phase eutectic colonies.[12] This kind of structure is barely seen in the equilibrium solidification of binary eutectic alloys; however, solute additions can promote instability at the planar liquid–solid interface, resulting in the formation of two-phase eutectic colonies.[13] The competition between primary and eutectic phases in alloys with eutectic composition is basically governed by the growth rate, v, and the presence of alloying elements (or impurities).

Depending on the soldering production conditions, wetting and flow characteristics of the Sn-0.7 wt.%Cu solder alloy can be unsatisfactory, due to poor penetration of plated-through holes and dull, grainy joints. A particular problem often found with Sn-0.7 wt.%Cu solder in wave soldering is bridging, which tends to be resistant to elimination by normal process optimization procedures such as higher bath temperatures. In practice, alloying additions of around 0.05% Ni to the Sn-0.7 wt.%Cu alloy have been reported to have significant beneficial effects on results obtained during wave soldering. Moreover, it has been noted that the addition of Ni to the Sn-0.7 wt.%Cu solder promotes the nucleation of fine uniform Cu_6Sn_5 intermetallic precipitates due to the higher solubility of Ni in Cu compared with that of Sn.[14] Ventura et al.[15] examined the addition of 0 ppm to 1000 ppm Ni to a Sn-0.7 wt.%Cu solder alloy. It was shown that Ni can significantly alter the microstructure of Sn-0.7Cu-xNi alloys. Ni additions were found to decrease the volumetric fraction of primary β-Sn dendrites. Maximum fluidity length measurements showed that the flow behavior of solidifying Sn-0.7Cu-xNi alloys is sensitive to small nickel additions. A peak in maximum fluidity length was measured at 500 ppm Ni.

According to Nogita,[7] there is some evidence that intermetallic layers in Ni-free Sn-Cu solders may experience more cracking than those that contain Ni. The authors stated that the stabilization of the hexagonal $(Cu,Ni)_6Sn_5$ phase in Ni-containing solder alloys may prevent volumetric changes that could contribute to cracking in Ni-free alloys. Moreover, Tsukamoto et al.[16] observed that Ni addition to Sn-Cu solders increases both the modulus of elasticity and hardness of the interface intermetallics.

The present study focuses on the effects of Ni additions up to 1000 ppm on the interfacial heat transfer coefficient (h_i), the growth rate (v), and the cooling rate ($\dot{T}$) of a eutectic Sn-0.7 wt.%Cu solder alloy solidified under non-steady-state conditions. The microstructural evolution as a function of these solidification thermal parameters is examined for both Ni-modified and unmodified Sn-0.7 wt.%Cu solders. Finally, the dependence of tensile strength and elongation to fracture on the cell/dendritic spacing is analyzed.

EXPERIMENTAL PROCEDURES

Details of the directional solidification assembly used in this study may be found in previous articles.[17,18] Heat is directionally extracted only through a water-cooled low-carbon-steel bottom, promoting vertical upward directional solidification. A stainless-steel split mold was used, having internal diameter of 60 mm, height of 157 mm, and wall thickness of 5 mm. The lateral inner mold surface was covered with a layer of insulating alumina to minimize radial heat losses. The bottom part of the mold was closed with a thin (3 mm) carbon-steel sheet. Ni-modified and unmodified Sn-0.7 wt.%Cu solder alloys were used in the experiments, which were performed under thermally and solutally stable solidification conditions.[9] The thermophysical properties used in the calculations are summarized in Table I.

In order to determine the compositions of the alloys, as-cast samples were machined and collected

chips were tested by inductively coupled plasma-optical emission spectrometry (ICP-OES). The chemistry of each alloy is presented in Table II.

Continuous temperature measurements in the casting were monitored during solidification via the output of a bank of fine type J thermocouples sheathed in 1.6 mm outside diameter (O.D.) stainless-steel tubes, positioned at different positions from the heat-extracting surface at the bottom of the casting. All thermocouples were connected by coaxial cables to a data logger interfaced with a computer, and the temperature data were acquired automatically.

The casting was sectioned along the longitudinal direction, and the macrostructure was revealed (2 mL HCl, 10 g $FeCl_3$, 100 mL H_2O). An etching solution of 92 vol.% CH_3OH, 5 vol.% HNO_3, and 3 vol.% HCl applied during 5 s was used to reveal the microstructure. Longer immersion times of about 40 s permitted the eutectic phase to be examined.

The triangle method was employed to measure both the primary dendritic arm spacing (λ_1) and the cellular spacing (λ_c) on transverse sections of the directionally solidified castings.[20] At least 40 measurements were performed for each selected position along the casting length. An optical image processing system (GX51; Olympus Co., Japan) was used to acquire the images.

Figure 1 shows a schematic representation indicating the positions along the casting length from where the specimens were extracted for the tensile tests. The transverse specimens were prepared according to specifications of ASTM Standard E 8M/04 and tested in an Instron 5500R machine at strain rate of about 1×10^{-3} s^{-1}. To ensure reproducibility of the tensile results, four specimens were tested for each selected position and both the ultimate tensile strength and elongation were determined for specimens extracted from different positions along the casting length. Microstructural characterization was performed using a field-emission gun (FEG) scanning electron microscope (SEM, XL30 FEG; Philips) coupled to an energy dispersive spectroscope (EDS, Oxford Link ISIS 300). Cross-sectional samples (10 mm × 10 mm, square-shaped) for XRD analyses were extracted from the central part of the castings and polished. The thicknesses of these samples were preserved for at least 3 mm. x-Ray diffraction (XRD) patterns were obtained by a Siemens D5000 diffractometer in the 2θ range from 20° to 90° using Cu K_α radiation with wavelength, λ, of 0.15406 nm.

Table I. Thermophysical properties of alloys used in the experimental analysis[12,19]

Properties	Symbol (units)	Sn-0.7 wt.%Cu
Thermal conductivity	k_S/k_L (W m^{-1} K^{-1})	67/33
Specific heat	c_S/c_L (J kg^{-1} K^{-1})	257/267
Density	ρ_S/ρ_L (kg m^{-3})	7166/6986
Latent heat of fusion	δH (J kg^{-1})	60,700
Melting temperature (Sn)	T_F (°C)	232
Eutectic temperature	T_E (°C)	227.1
Eutectic composition	C_{eut} (wt.%)	0.7

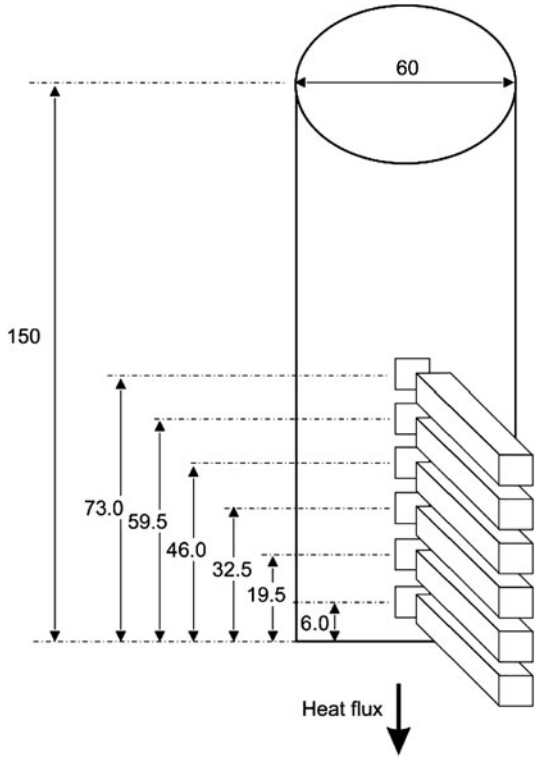

Fig. 1. Schematic representation of positions from the cooled bottom of the Sn-Cu(-Ni) alloy castings from where the specimens for tensile tests were extracted (dimensions in mm).

Table II. Compositions of the as-cast Sn-Cu alloys, as determined by ICP-OES (wt.%)

Alloy	Chemical composition (wt.%)								
	Sn	Cu	Ni	Ag	Pb	Sb	Zn	Al	Fe
Sn-0.7 wt.%Cu	Bal.	0.69	<0.002	<0.003	0.029	<0.007	<0.002	<0.002	0.004
Sn-0.7 wt.%Cu-0.05 wt.%Ni	Bal.	0.68	0.050	<0.006	0.037	<0.007	<0.001	<0.002	0.006
Sn-0.7 wt.%Cu-0.1 wt.%Ni	Bal.	0.68	0.100	<0.005	0.038	<0.007	<0.001	<0.002	0.006

RESULTS AND DISCUSSION

Figure 2 shows the resulting experimental cooling curves for the thermocouples inserted in the Sn-0.7 wt.%Cu, Sn-0.7 wt.%Cu-0.05 wt.%Ni, and Sn-0.7 wt.%Cu-0.1 wt.%Ni alloy castings. The simulations obtained by a finite-difference solidification heat flow program[21] were compared with these experimental thermal data. An automatic search was used to select the best theoretical–experimental fits from a range of transient interfacial heat transfer coefficient (h_i) profiles, as described in previous articles.[21,22] Experimental power laws relating h_i with time were derived and are also shown in Fig. 2d. Recently, it has been demonstrated that h_i varies in time according to an expression of the form $h_i = at^{-m}$, where a (multiplier) and m (exponent) are constants and $m < 0.5$.[21]

The thermophysical properties, the solidification range, and the melt fluidity are known to be important factors affecting h_i. Rosa et al.[23] found different multipliers for the power laws characterizing the variation of h_i during the course of upward directional solidification of Pb-Sb alloys. The authors stated that such multipliers are mainly linked to the wettability of the liquid layer in contact with the mold inner surface, i.e., related to the fluidity of the molten alloy. A correlation between the multiplier a and the fluidity has been established, with higher a values corresponding to the two extremes of the hypoeutectic range of the compositions examined, i.e., pure Pb and the eutectic composition. Regarding the present results obtained with Ni modification, small additions of 500 ppm and 1000 ppm Ni to the eutectic Sn-0.7 wt.%Cu alloy were shown to be enough to increase significantly the multiplier a, as shown in Fig. 2d, indicating improvement of the alloy wettability by modification with Ni.

The readings of the thermocouples were also used to generate a plot of position from the metal/mold interface as a function of time corresponding to the eutectic front passing by each thermocouple. A curve-fitting technique applied to these experimental points yielded a power function of position

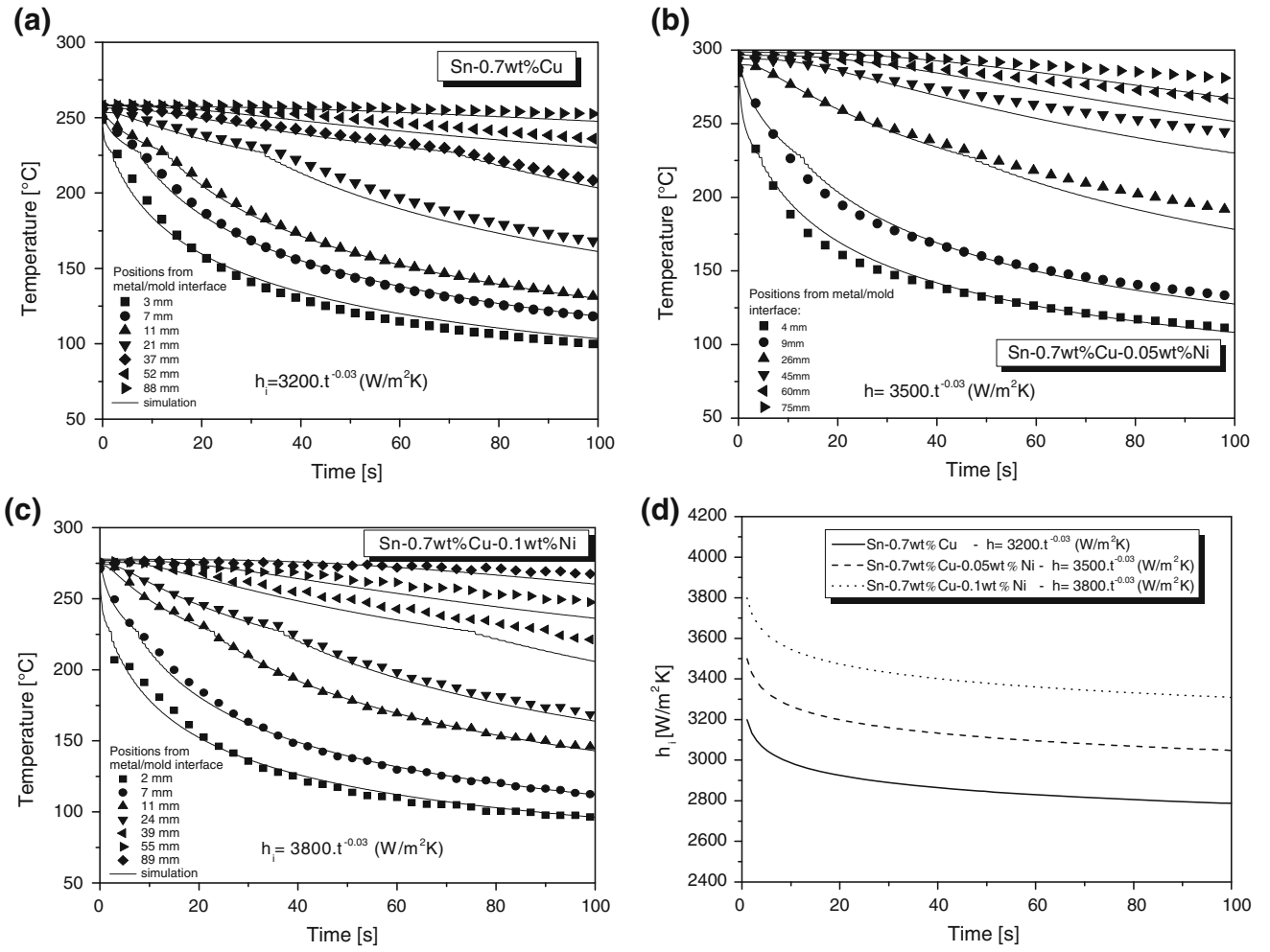

Fig. 2. Experimental cooling curves and simulations of the transient h_i profiles for: (a) Sn-0.7 wt.%Cu, (b) Sn-0.7 wt.%Cu-0.05 wt.%Ni, and (c) Sn-0.7 wt.%Cu-0.1 wt.%Ni alloys.

varying with time. The derivative of this function with respect to time gave values for the eutectic growth velocity, v. Figure 3a, c, e shows the experimental evolutions of v for the experimentally examined alloys together with the simulated results. The experimental cooling rate (Fig. 3b, d, f) was determined by considering the thermal data recorded immediately after the passage of the

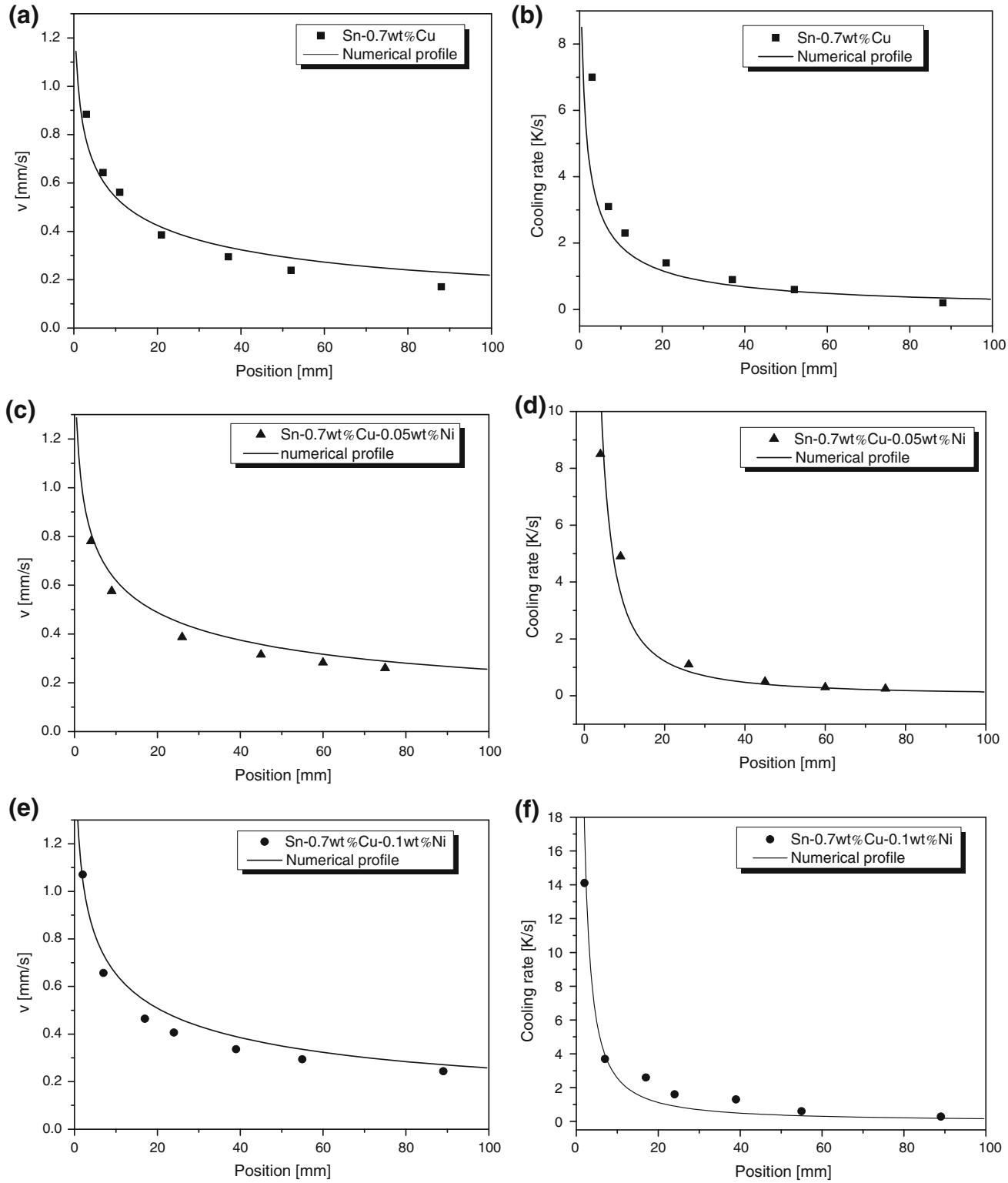

Fig. 3. Simulated and experimental values of eutectic (a, c, e) growth rate, and (b, d, f) cooling rate for the Sn-0.7 wt.%Cu, Sn-0.7 wt.%Cu-0.05 wt.%Ni, and Sn-0.7 wt.%Cu-0.1 wt.%Ni alloys.

eutectic front by each thermocouple. The good fit between the numerical and experimental results, as observed in Fig. 3, allows the numerical growth rates and cooling rates to be used to establish correlations with microstructure parameters at positions in castings where thermocouples had not been inserted.

Figures 4 and 5 show the macrostructures of the three examined alloy castings and some typical transverse microstructures obtained after metallographic examination, respectively. Columnar grains prevailed along the entire length of the solidified castings, which means that vertically aligned grains have grown from the bottom of the casting.

Coarser eutectic cells characterize positions farther from the metal/mold interface for the three cases examined, as can be seen in Fig. 5. Lower cooling rates can be related to coarser microstructures. The influence of thermal parameters such as the cooling rate translates to the experimental determined values of λ_c.

Figure 6 shows the evolution of both the cellular and primary dendritic arm spacings as a function of cooling rate (a, c, e) and growth rate (b, d, f) for the Sn-0.7 wt.%Cu, Sn-0.7 wt.%Cu-0.05 wt.%Ni, and Sn-0.7 wt.%Cu-0.1 wt.%Ni alloys, respectively. In the case of the nonmodified alloy, a gradual cellular to dendritic transition was observed to occur for cooling rates ranging from 0.9 K/s to 1.5 K/s and for growth rates from 0.3 mm/s to 0.5 mm/s. This is in agreement with a study of cellular/dendritic transition for a Sn-Pb alloy, which was reported to occur along a range of cooling rates from 0.5 K/s to 5.2 K/s.[17] In contrast, an abrupt cellular to dendritic transition occurred when a cooling rate of about 6.0 K/s was achieved during directional solidification of both Sn-0.7 wt.%Cu-0.05 wt.%Ni and Sn-0.7 wt.%Cu-0.1 wt.%Ni alloys. The growth rate associated with the cellular-to-dendritic transition was roughly the same for these alloys (about 0.8 mm/s). This seems to indicate that small additions of Ni tend to stabilize the growth of cells, even for higher cooling rates or growth rates, compared with the microstructure evolution of the Sn-0.7 wt.%Cu alloy. These results seem to agree with the experimental observations reported by Ventura et al.,[15] who stated that Ni can significantly alter the microstructure of Sn-0.7 Cu-xNi alloys, decreasing the volumetric fraction of primary β-Sn dendrites.

It can be seen that the exponents -0.55 and -1.1 properly represent the growth of the two-phase eutectic cells as a function of the cooling rate and growth rate, respectively, for all alloys examined. These eutectic two-phase cells are also known as eutectic colonies. Solute additions can make the planar liquid–solid interface unstable, resulting in the formation of eutectic colonies. The competition between primary and eutectic phases in alloys with eutectic composition is basically governed by the growth rate, v, and the presence of impurities. Addition of 500 ppm or 1000 ppm Ni seems to extend the range of cellular growth, inhibiting the presence of dendrites, which were confined only to the very early positions in the casting (>6.0 K/s).

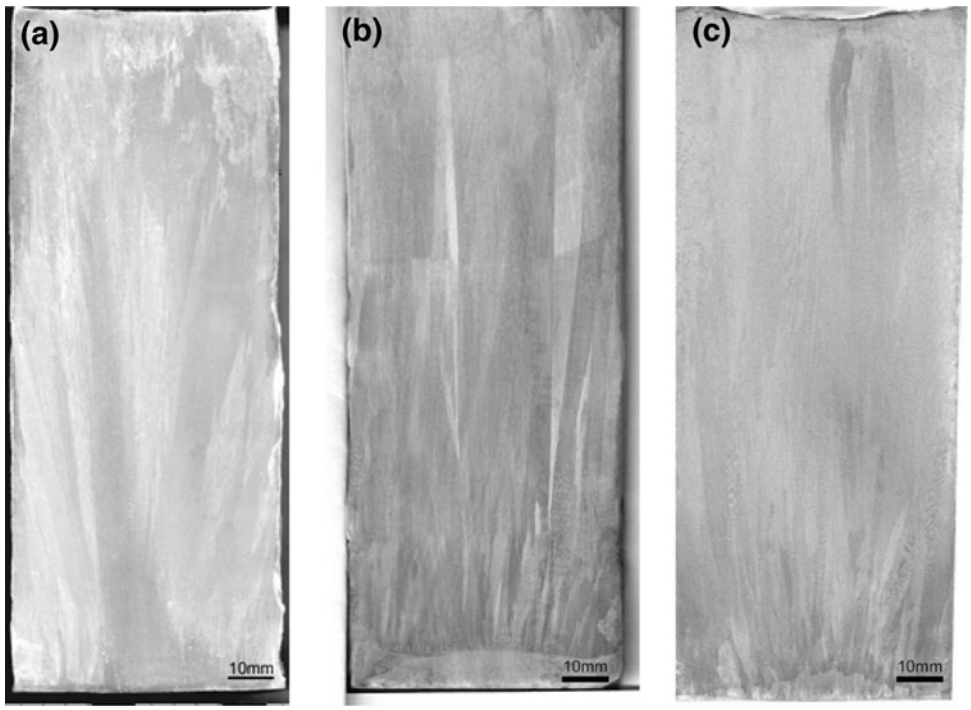

Fig. 4. Macrostructures of: (a) Sn-0.7 wt.%Cu, (b) Sn-0.7 wt.%Cu-0.05 wt.%Ni, and (c) Sn-0.7 wt.%Cu-0.1 wt.%Ni alloy castings.

Three experimental equations were found to fit the experimental scatters of cell and primary dendritic spacings with the cooling rate for the three examined alloys (Fig. 6a, c, e). The cell spacing increases with the microaddition of Ni to the Sn-0.7 wt.%Cu alloy. A higher Ni content induces further increase in λ_c. A similar effect can also be observed in Fig. 6b, d, f for the variation in the microstructural spacing as a function of growth rate. However, a single experimental power law: $\lambda_c = 33(v)^{-1.1}$ can generate the experimental scatters for both additions of Ni: 500 ppm and 1000 ppm.

Figure 7 depicts details regarding the microstructure transitions observed for all the alloys experimentally examined. Microstructure features and the corresponding growth rates and cooling rates are also included. Figure 7a refers to a cross-section of the nonmodified Sn-Cu alloy casting at 20 mm from the casting cooled surface. In this case, the presence of both cellular and dendritic morphologies characterized a transition region which prevails for 15 mm along the casting length. The two other cases, with small Ni additions, permitted an abrupt transition to be observed without a transition zone.

Figure 8 shows the experimental macrosegregation profile of Cu along the directionally solidified casting. It can be seen that, despite the well-known tendency for an inverse macrosegregation profile for alloys having Cu as the main solute,[24] it can be seen that only the casting surface has a slightly higher Cu concentration; i.e., the mean Cu composition of the tensile specimens along the casting length can be considered essentially constant. Since the Ni content was even lower (maximum of 1000 ppm) it is very unlikely that a Ni compositional difference along the casting lengths could significantly affect the resulting mechanical properties.

It is well known that the morphology, size, and distribution of stable and metastable intermetallic particles may affect the mechanical properties of Sn-Cu alloys.[14,16] In order to examine features of the intermetallic particles and the eutectic phase, SEM images were obtained in the present study after deep chemical etching of the samples. Figure 9 shows three typical SEM micrographs of the Sn-0.7 wt.%Cu-0.1 wt.%Ni alloy. Local analyses, especially regarding the composition of some isolated particles, were performed by an EDS microprobe. Positions in the casting at 5 mm and 30 mm

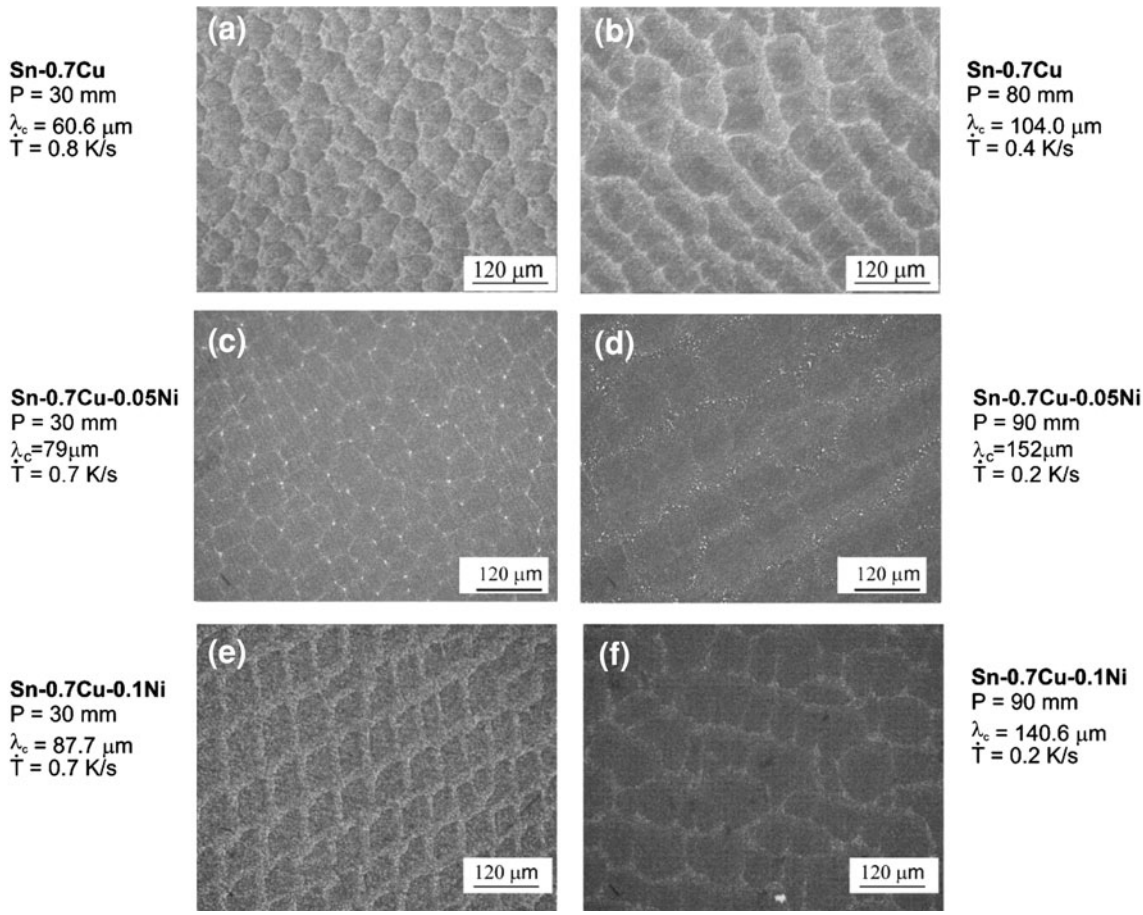

Fig. 5. Typical as-cast microstructures along the castings lengths highlighting the eutectic cell spacing and the corresponding cooling rate for: (a, b) Sn-0.7 wt.%Cu, (c, d) Sn-0.7 wt.%Cu-0.05 wt.%Ni, and (e, f) Sn-0.7 wt.%Cu-0.1 wt.%Ni alloys.

from the metal/mold interface were chosen to perform this examination, since they are associated with quite different solidification thermal parameters (Fig. 3). The simultaneous presence of both $(Cu,Ni)_6Sn_5$ and Ni_3Sn_4 primary intermetallics can be observed only for the early positions in the casting (up to 5 mm), as shown in Fig. 9a. This occurs only for Ni-modified Sn-Cu alloys with lower amount of these intermetallics (alloy having 500 ppm Ni). The presence of Ni in the Sn-0.7 wt.%Cu-0.1 wt.%Ni alloy may be confirmed by the tables depicted in Fig. 9a, b. Growth of primary

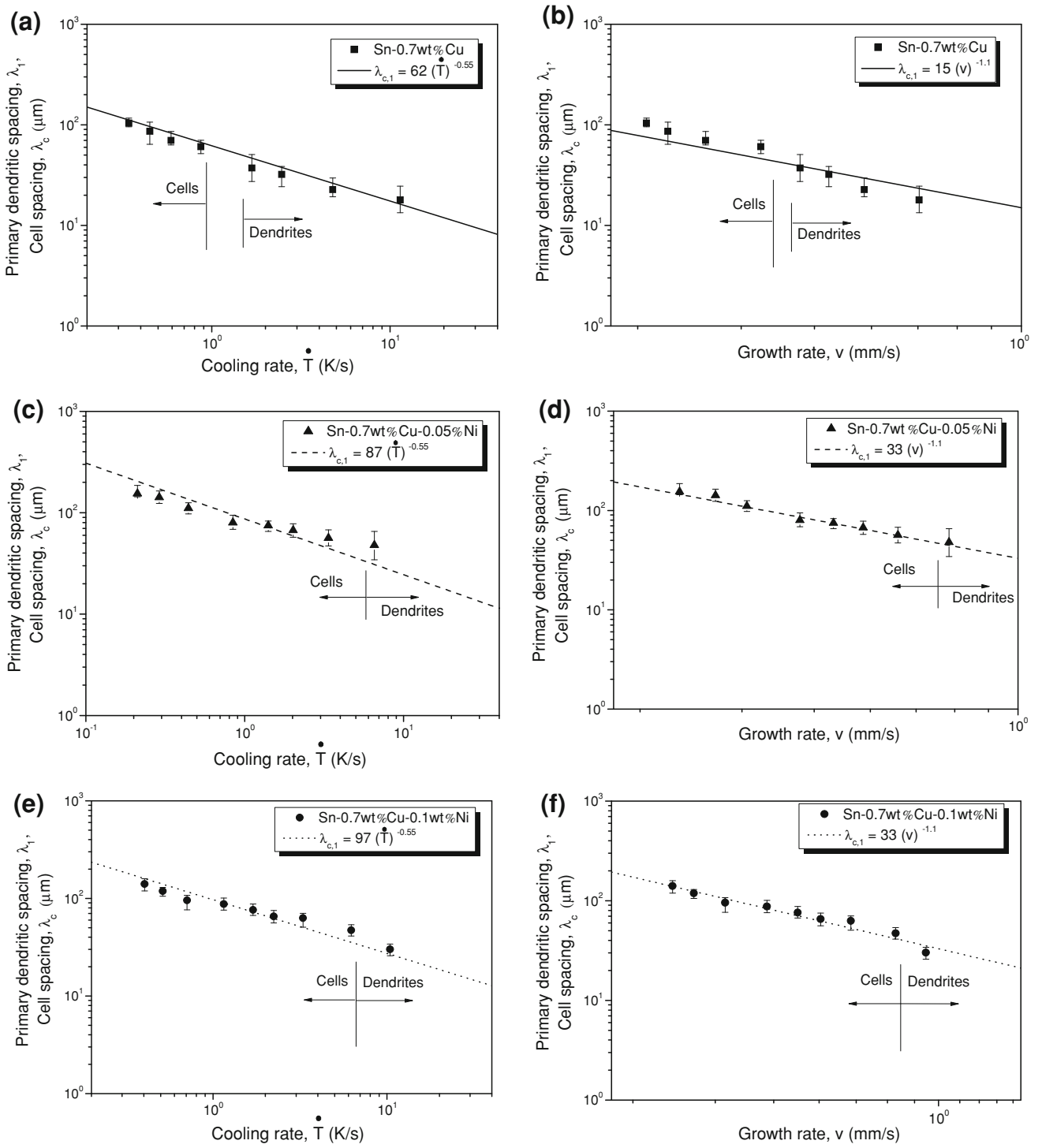

Fig. 6. Evolution of eutectic cell (λ_c) and primary dendritic spacing (λ_1) with the cooling rate, $\dot{T}$ (a, c, e) and with the growth rate, v (b, d, f) for the Sn-0.7 wt.%Cu, Sn-0.7 wt.%Cu-0.05 wt.%Ni, and Sn-0.7 wt.%Cu-0.1 wt.%Ni alloys, respectively.

intermetallics was not observed along the entire nonmodified Sn-Cu alloy casting.

According to Wang and Chen,[25] Cu_6Sn_5 and Ni_3Sn_4 intermetallics are the two predominant reaction phases regarding industrial applications of Sn-Cu solder alloys. Depending upon the Cu concentration, both intermetallics can be formed at Sn-Cu/Ni contacts.[25] Wang and Shen[26] stated that, with 0.05 wt.% Ni addition to the Sn-0.7 wt.%Cu alloy, the Cu_6Sn_5 phase changes from rod shaped to large faceted crystals, which can be characterized by H-shaped or M-shaped cross sections. Some of them can be observed in Fig. 9a, appearing to grow from a central point before separating into distinct branches. In a recent study, Gourlay et al.[27] carried out near-steady-state unidirectional solidification experiments with a Sn-0.7 wt.%Cu-0.06 wt.%Ni alloy, deducing the solidification sequence by using a synchrotron x-ray radiography facility. According to this study, primary nonbranched $(Cu,Ni)_6Sn_5$ intermetallics may develop ahead of the eutectic front during growth. This was also found in the present investigation, especially along the early casting positions. These authors also stated that the primary intermetallics had a Ni content which was higher than that of the eutectic $(Cu,Ni)_6Sn_5$ particles. Such ternary phase can be formed when Ni atoms take some positions of Cu in the Cu_6Sn_5 structure. As can be seen in Fig. 9a (see higher-magnification detail at the left side), the Ni_3Sn_4 intermetallic has a needle-like morphology characterized by a large number of facets. The Ni content (3.96 at.%) obtained for the large faceted particle seen in Fig. 9a is fairly close to the typical Ni content found for the $(Cu,Ni)_6Sn_5$ intermetallic, which is about 5.0 at.% Ni.[7] However, a smaller quantity of Ni was obtained by the local elemental measurement, as shown in Fig. 9b. This is due to the fact that in this case the microprobe was positioned aligned with the Sn-rich matrix. In this specific region the prevalent microstructure is mainly formed by very fine and uniform eutectic intermetallics dispersed in a Sn-rich matrix. A previous study in the literature[27]

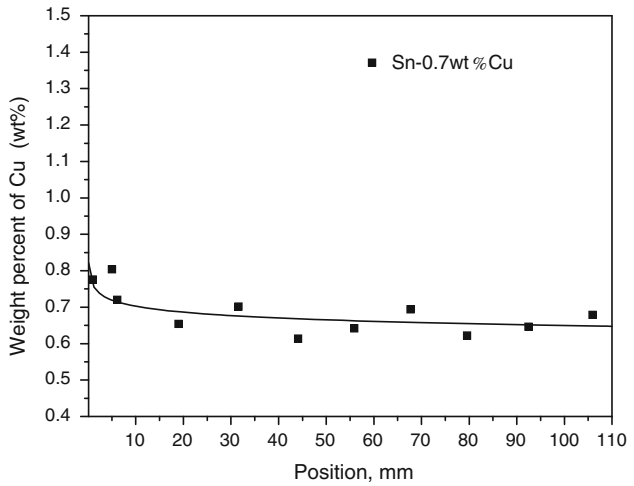

Fig. 8. Experimental macrosegregation profile obtained for the Sn-0.7 wt.%Cu alloy.

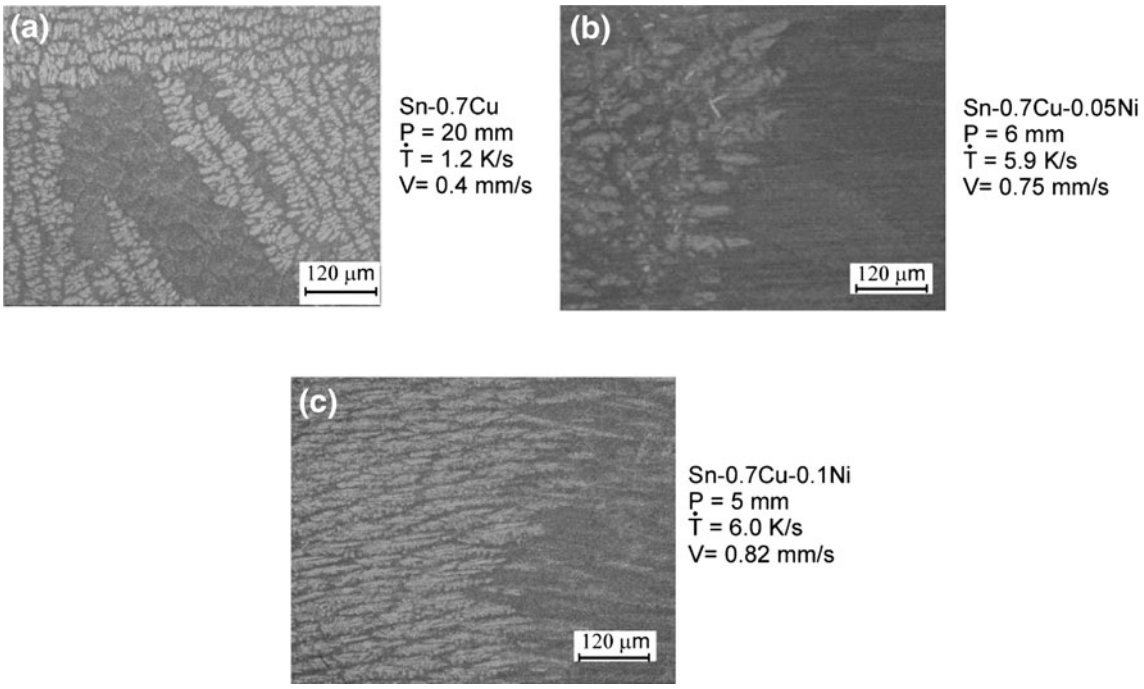

Fig. 7. Detailed optical images showing the limits between eutectic cells and dendrites for (a) Sn-0.7 wt.%Cu (cross section), (b) Sn-0.7 wt.%Cu-0.05 wt.%Ni (longitudinal section), and (c) Sn-0.7 wt.%Cu-0.1 wt.%Ni alloys (longitudinal section).

reported that smaller Ni contents may characterize such regions.

Eutectic rod-like particles with very low Ni content prevailed at 30 mm. The corresponding composition can be confirmed by the table shown in Fig. 9b. The microstructure is mainly formed by fine and uniform eutectic intermetallics dispersed in a Sn-rich matrix. A higher-magnification detail of this microstructural arrangement is depicted on the left side of Fig. 9b.

XRD patterns of the Sn-Cu (Ni) alloys (Fig. 10) were obtained to complement the EDS compositional analysis shown in Fig. 9. The samples examined in the present study exhibit the presence of peaks associated with Sn, Cu_6Sn_5, $(Cu,Ni)_6Sn_5$, and Ni_3Sn_4 phases. Five different positions were examined along each Sn-Cu (Ni) alloy casting, encompassing a representative range of cooling rates. There were no clear tendencies regarding the intensities of peaks for the different positions from the casting cooled surface. Thus, a definitive evaluation of the intensities of peaks as a function of tip cooling rate cannot be established. However, for the Sn-0.7 wt.%Cu-0.1 wt.%Ni alloy casting, the presence of a higher fraction of phases containing Ni, such as Ni_3Sn_4 and $(Cu,Ni)_6Sn_5$, can be noted for positions closer to the casting cooled surface due to the higher concentration of Ni at these locations. The trace-level Ni addition to the eutectic or near-eutectic Sn-Cu stabilized the hexagonal η-$(Cu,Ni)_6Sn_5$ phase, as stated by Nogita.[7] The $(Cu,Ni)_6Sn_5$ peaks present in the XRD patterns confirmed that this phase has a hexagonal structure at room temperature, especially when comparing the characteristic peaks with those provided by Nogita.[7]

The traditional Hall–Petch equation focuses on the relationship between grain size and mechanical properties, which means that the influence of any parameters other than the grain boundary is not included in the analysis. However, deeper examination within individual grains reveals the presence of cellular or dendritic networks of continuously varying solute content, second phases, and possibly porosity and inclusions, which cannot be neglected, since these parameters can have a significant influence on the final properties. The present work proposes to include the effect of cellular (λ_c) or dendritic (λ_1) spacings by modifying the classical Hall–Petch relationship ($\sigma = \sigma_0 + kd^{-1/2}$) with d (mean grain size) being replaced with λ_c and λ_1. Figure 11a, b depicts the experimental correlations found for ultimate tensile strength (σ_u) and elongation (δ) as a function of cellular/primary spacing, respectively. The addition of 1000 ppm Ni permitted higher σ_u and lower δ to be obtained. Since the dendritic

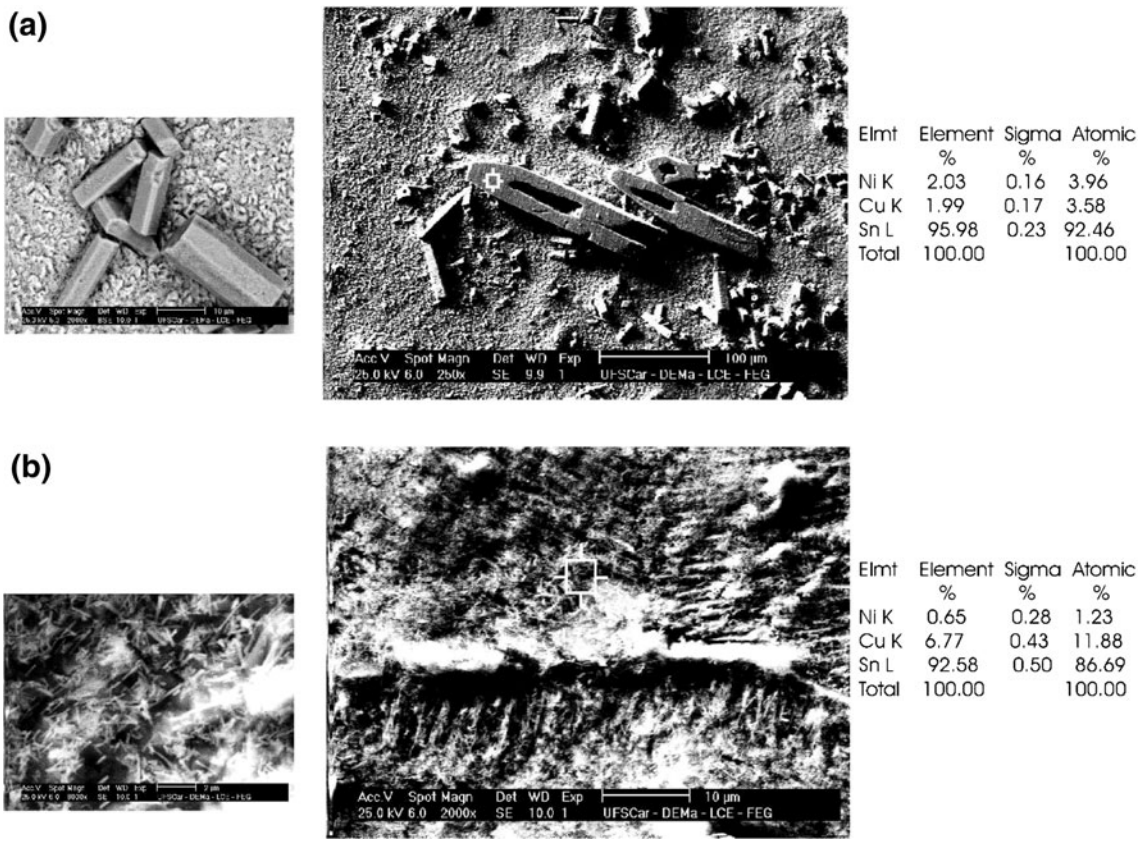

Fig. 9. SEM microstructures and EDS results for the Sn-0.7 wt.%Cu-0.1 wt.%Ni alloy at positions: (a) 5 mm and (b) 30 mm from the casting surface.

microstructure, found in the cases of the Ni-modified alloys, was restricted only to the region closer to the casting cooled surface, it was totally removed during machining of the first extracted tensile specimen. This limited the correlation between the mechanical properties of the Sn-0.7 wt.%Cu-0.05 wt.%Ni and Sn-0.7 wt.%Cu-0.1 wt.%Ni alloys and the microstructural spacing only to the range of cellular growth. A single Hall–Petch-type correlation is able to represent both experimental scatters of σ_u found for these alloys, as can be seen in Fig. 11a. The presence of hard and brittle intermetallic particles was detected only in the early regions with occurrence of cells (Fig. 9a). High σ_u values have been obtained, associated with finer eutectic cells for both the Sn-0.7 wt.% Cu-0.05 wt.%Ni and Sn-0.7 wt.%Cu-0.1 wt.%Ni alloys. These results can be considered adequate as they are slightly higher than that of the eutectic Sn-0.6 wt.%Cu-0.05 wt.%Ni solder alloy tested by Tetsuro,[28] i.e., σ_u of 33 MPa. The Ni-modified solder alloys of the present study meet strength requirements if compared with the results reported by Chen et al.,[29] who evaluated the tensile mechanical properties of Ni-Sn-0.7 wt.%Cu-Ni joints. These joints exhibited ultimate tensile strength of 31 MPa. Preferential nucleation of Sn-Cu particles was also reported by Nimmo,[14] who similarly incorporated Ni to form the Sn-0.7 wt.%Cu alloy composition. In all alloys examined, σ_u increases with decreasing $\lambda_{1,c}$, while opposite trends are observed for the elongation.

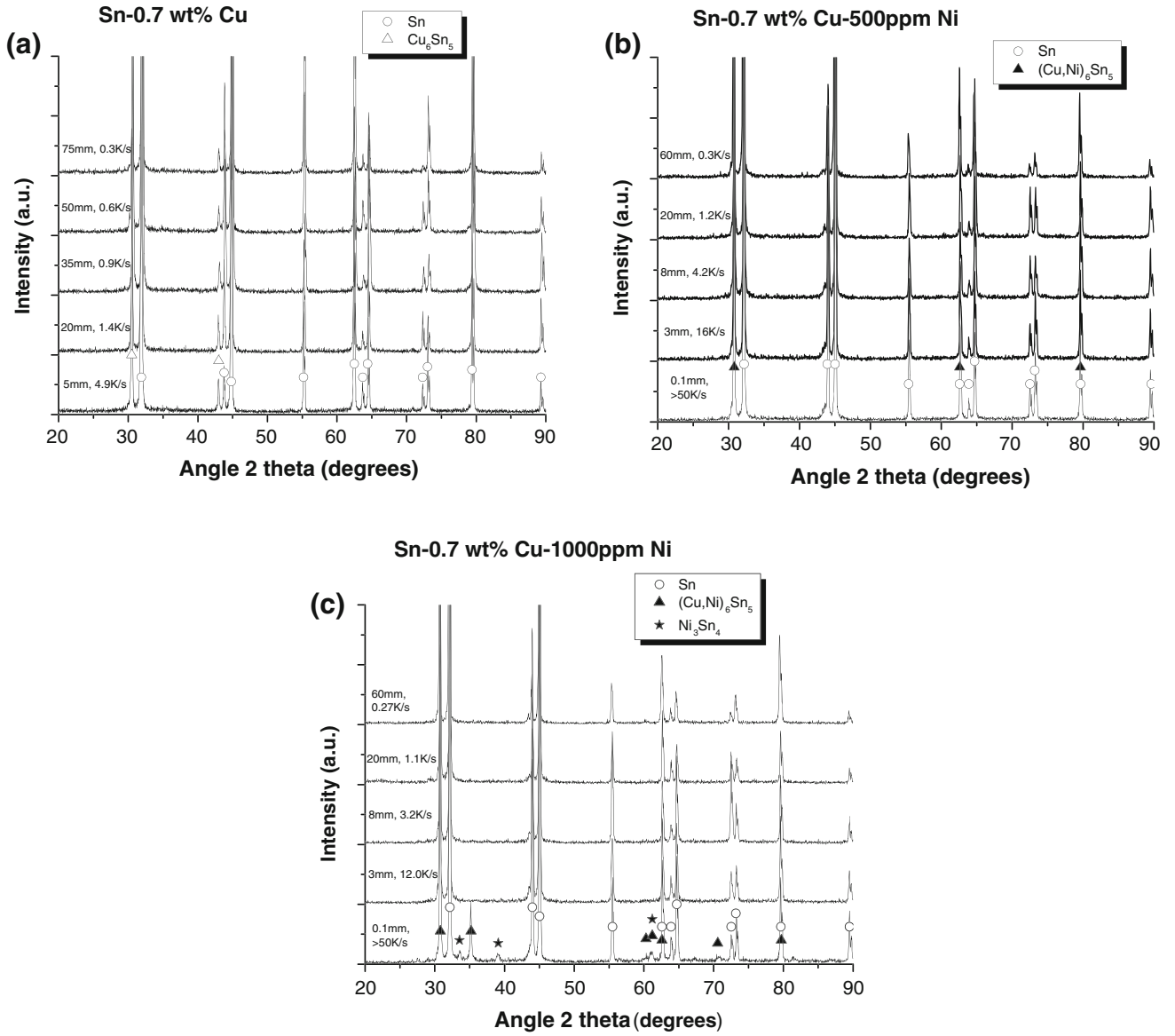

Fig. 10. Typical XRD patterns of (a) Sn-0.7 wt.%Cu, (b) Sn-0.7 wt.%Cu-0.05 wt.%Ni, and (c) Sn-0.7 wt.%Cu-0.1 wt.%Ni alloys for different positions along the casting length.

The more enlarged dendritic region observed in the Sn-0.7 wt.%Cu alloy permitted the evaluation of the effects of this morphology on σ_u. In fact, an essentially constant value of about 25 MPa was found, even for the case of regions with more refined dendritic arrangements. Cells and dendrites very close in size permit a same level of mechanical strength to be attained.

While a classical Hall–Petch-type correlation ($\sigma_u = \sigma_{u0} + K\lambda_c^{-1/2}$) was able to fit the experimental scatters of the Sn-0.7 wt.%Cu-0.05 wt.%Ni and Sn-0.7 wt.%Cu-0.1 wt.%Ni alloys, an alternative approach ($\sigma_u = \sigma_{u0} + K_1\lambda_{1,c}^{-1/2} - K_2\lambda_{1,c}$) was shown to be more adequate to represent that of the Sn-0.7 wt.%Cu alloy. Although similar ultimate tensile strengths were obtained for both levels of Ni alloying, higher elongations were found for the Sn-Cu alloy with 500 ppm Ni. This may be due to the slightly finer eutectic cells obtained in this case, associated with a considerable lower content of brittle and coarse Sn-Cu-Ni intermetallics. The Hall–Petch-type expression derived for the elongation of the Sn-0.7 wt.%Cu alloy lay between those proposed for the two Ni-modified alloys.

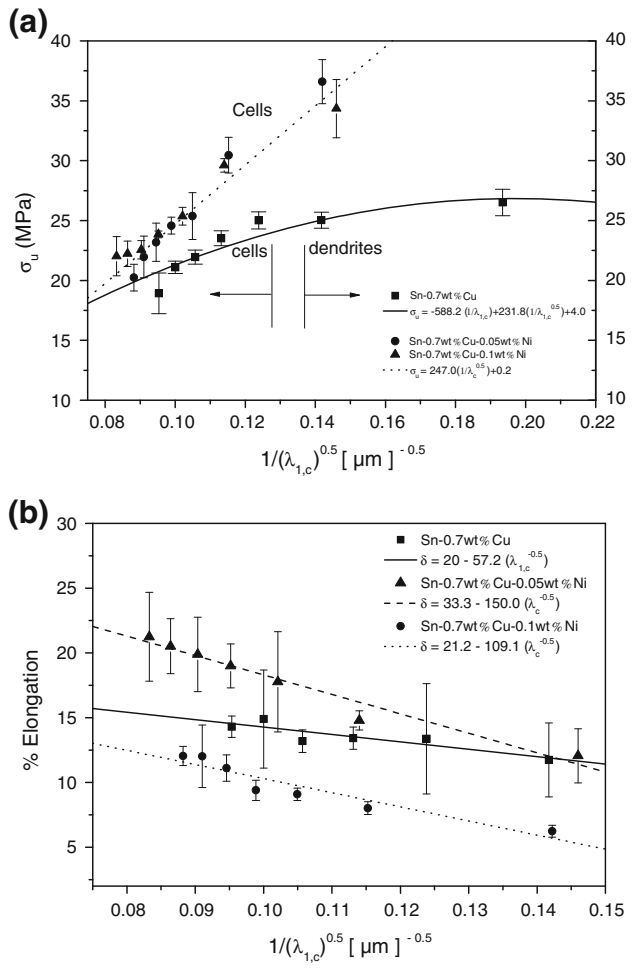

Fig. 11. (a) Ultimate tensile strength (σ_U) and (b) elongation (δ) as a function of primary dendritic/cell spacing ($\lambda_{1,c}$) for the Ni-modified and unmodified Sn-0.7 wt.%Cu alloys.

CONCLUSIONS

The following conclusions can be drawn from the present experimental investigation:

- The present results of interfacial heat transfer coefficients show that small additions of 500 ppm and 1000 ppm Ni to the composition of a eutectic Sn-0.7 wt.%Cu solder alloy are enough to promote considerable improvements in alloy wettability.
- The microstructure of the Sn-0.7 wt.%Cu(-Ni) alloys was shown to be characterized by cellular and dendritic matrices. In the case of the non-modified alloy, a gradual cellular to dendritic transition was observed to occur for cooling rates ranging from 0.9 K/s to 1.5 K/s. In contrast, an abrupt cellular to dendritic transition occurred when a cooling rate of about 6.0 K/s was achieved during directional solidification of both Sn-0.7 wt.%Cu-0.05 wt.%Ni and Sn-0.7 wt.%Cu-0.1 wt.%Ni alloys. These figures indicate that small additions of Ni tend to stabilize the growth of cells. Experimental growth laws relating cellular/dendritic spacings to the cooling rate and the growth rate are proposed.
- Simultaneous presence of both $(Cu,Ni)_6Sn_5$ and Ni_3Sn_4 primary intermetallics for the Ni-modified alloys was observed only for positions in the casting up to 5 mm from the cooled surface, i.e., associated with the highest range of cooling rates.
- Higher ultimate tensile strengths (σ_u) were shown to be associated with finer eutectic cells for both the Sn-0.7 wt.%Cu-0.05 wt.%Ni and Sn-0.7 wt.%Cu-0.1 wt.%Ni alloys. Experimental Hall–Petch-type equations correlating σ_u and the elongation with the cell spacing are proposed.
- The proposed experimental equations can be used in the control of the soldering process of both Ni-modified and unmodified Sn-0.7 wt.%Cu alloys by manipulating the cooling rate in the preprogramming of desired microstructural arrangements as well as of expected levels of strength and ductility.

ACKNOWLEDGEMENTS

The authors acknowledge financial support by FAPESP (The Scientific Research Foundation of the State of São Paulo, Brazil), CNPq (The Brazilian Research Council), and IFSP.

REFERENCES

1. L.R. Garcia, W.R. Osório, L.C. Peixoto, and A. Garcia, *Mater. Charact.* 61, 212 (2010).
2. J. Chen, J. Shen, D. Min, and C.F. Peng, *J. Mater. Sci.* 20, 1112 (2009).
3. Y. Li, K.-S. Moon, and C.P. Wong, *Science* 308, 1419 (2005).
4. E. Çadırlı, U. Böyük, S. Engin, H. Kaya, N. Maraslı, and A. Ülgen, *J. Alloys Compd.* 486, 199 (2009).

5. L.R. Garcia, W.R. Osório, L.C. Peixoto, and A. Garcia, *J. Electron. Mater.* 38, 2405 (2009).
6. G. Li, Y. Shi, H. Hao, Z. Xia, Y. Lei, and F. Guo, *J. Alloys Compd.* 491, 382 (2010).
7. K. Nogita, *Intermetallics* 18, 145 (2010).
8. K.G. Snowdon, C.G. Tanner, J.R. Thompson, *Proceedings of 50th ECTC*, Las Vegas, NV (Piscataway, NJ: IEEE, 2000), p. 1416.
9. J.E. Spinelli, D.M. Rosa, I.L. Ferreira, and A. Garcia, *Mater. Sci. Eng. A* 383, 271 (2004).
10. P. Donelan, *Mater. Sci. Technol.* 16, 261 (2000).
11. P.R. Goulart, J.E. Spinelli, N. Cheung, and A. Garcia, *Mater. Chem. Phys.* 119, 272 (2010).
12. I.T.L. Moura, C.L.M. Silva, N. Cheung, P.R. Goulart, A. Garcia, and J.E. Spinelli, *Mater. Chem. Phys.* 132, 203 (2012).
13. N. Tewari, S.V. Raj, and I.E. Locci, *Met. Mater. Trans.* 35A, 1632 (2004).
14. K. Nimmo, *Lead-Free Soldering in Electronics*, ed. K. Suganuma, chap. 3 (New York: Marcel Dekker Inc., 2004).
15. T. Ventura, C.M. Gourlay, K. Nogita, T. Nishimura, M. Rappaz, and A.K. Dahle, *J. Electron. Mater.* 37, 32 (2008).
16. H. Tsukamoto, Z. Dong, H. Huang, T. Nishimura, and K. Nogita, *Mater. Sci. Eng. B* 164, 44 (2009).
17. O.L. Rocha, C.A. Siqueira, and A. Garcia, *Mater. Sci. Eng. A* 347, 59 (2003).
18. A.P. Silva, J.E. Spinelli, N. Mangelinck-Noel, and A. Garcia, *Mater. Des.* 31, 4584 (2010).
19. T. Chellaih, G. Kumar, and N. Prabhu, *Mater. Des.* 28, 1006 (2007).
20. M. Gunduz and E. Çardili, *Mater. Sci. Eng. A* 327, 167 (2002).
21. N. Cheung, N.S. Santos, J.M.V. Quaresma, G.S. Dulikravich, and A. Garcia, *Int. J. Heat Mass Transf.* 52, 451 (2009).
22. I.L. Ferreira, J.E. Spinelli, J.E. Pires, and A. Garcia, *Mater. Sci. Eng. A* 408, 317 (2005).
23. D.M. Rosa, J.E. Spinelli, I.L. Ferreira, and A. Garcia, *Metall. Mater. Trans.* 39A, 2161 (2008).
24. I.L. Ferreira, C.A. Santos, V.R. Voller, and A. Garcia, *Metall. Mater. Trans.* 35B, 285 (2004).
25. C. Wang and S. Chen, *Acta Mater.* 54, 247 (2006).
26. C.H. Wang and H.T. Shen, *Intermetallics* 18, 616 (2010).
27. C.M. Gourlay, K. Nogita, A.K. Dahle, Y. Yamamoto, K. Uesugi, T. Nagira, M. Yoshiya, and H. Yasuda, *Acta Mater.* 59, 4043 (2011).
28. T. Nishimura, U.S. patent 6,180,055 B1 (2001).
29. S. Chen, S. Lee, and M. Yip, *J. Electron. Mater.* 32, 1284 (2003).